ACS APPLIED MATERIALS & INTERFACES

Research Article

Cite This: ACS Appl. Mater. Interfaces 2019, 11, 44474−44486

www.acsami.org

Highly Efficient Deep-Blue Electroluminescence Based on a Solution-Processable A−π−D−π−A Oligo(*p*-phenyleneethynylene) Small Molecule

Hakan Usta,*[,†] Dilek Alimli,[‡] Resul Ozdemir,[†] Salih Dabak,[§] Yunus Zorlu,[‡] Fahri Alkan,[†] Emine Tekin,[§] and Ayse Can[†]

[†]Department of Materials Science and Nanotechnology Engineering, Abdullah Gül University, 38080 Kayseri, Turkey

[‡]Department of Chemistry, Gebze Technical University, 41400 Gebze, Kocaeli, Turkey

[§]The Scientific and Technological Research Council of Turkey (TUBITAK)-Marmara Research Center (MAM), 41470 Gebze, Kocaeli, Turkey

Supporting Information

ABSTRACT: The development of solution-processable fluorescent small molecules with highly efficient deep-blue electroluminescence is of growing interest for organic light-emitting diode (OLED) applications. However, high-performance deep-blue fluorescent emitters with external quantum efficiencies (EQEs) over 5% are still scarce in OLEDs. Herein, a novel highly soluble oligo(*p*-phenyleneethynylene)-based small molecule, 1,4-bis((2-cyanophenyl)ethynyl)-2,5-bis(2-ethylhexyloxy)benzene (2EHO−CNPE), is designed, synthesized, and fully characterized as a wide band gap (2.98 eV) and highly fluorescent (Φ_{PL} = 0.90 (*solution*) and 0.51 (*solid-state*)) deep-blue emitter. The new molecule is functionalized with cyano (-CN)/2-ethylhexyloxy (-$OCH_2CH(C_2H_5)C_4H_9$) electron-withdrawing/-donating substituents, and ethynylene is used as a π-spacer to form an acceptor (A)−π−donor (D)−π−acceptor (A) molecular architecture with hybridized local and charge transfer (HLCT) excited states. Physicochemical and optoelectronic characterizations of the new emitter were performed in detail, and the single-crystal structure was determined. The new molecule adopts a nearly coplanar π-conjugated framework packed via intermolecular "C−H···π" and "C−H···N" hydrogen bonding interactions without any π−π stacking. The OLED device based on 2EHO−CNPE shows an EQE_{max} of 7.06% (EQE = 6.30% at 200 cd/m^2) and a maximum current efficiency (CE_{max}) of 5.91 cd/A (CE = 5.34 cd/A at 200 cd/m^2) with a deep-blue emission at CIE of (0.15, 0.09). The electroluminescence performances achieved here are among the highest reported to date for a solution-processed deep-blue fluorescent small molecule, and, to the best of our knowledge, it is the first time that a deep-blue OLED is reported based on the oligo(*p*-phenyleneethynylene) π-framework. TDDFT calculations point to facile reverse intersystem crossing (RISC) processes in 2EHO−CNPE from high-lying triplet states to the first singlet excited state ($T_2/T_3 \rightarrow S_1$) (*hot-exciton channels*) that enable a high radiative exciton yield ($\eta_r \sim 69\%$) breaking the theoretical limit of 25% in conventional fluorescent OLEDs. These results demonstrate that properly designed fluorescent oligo(*p*-phenyleneethynylenes) can be a key player in high-performance deep-blue OLEDs.

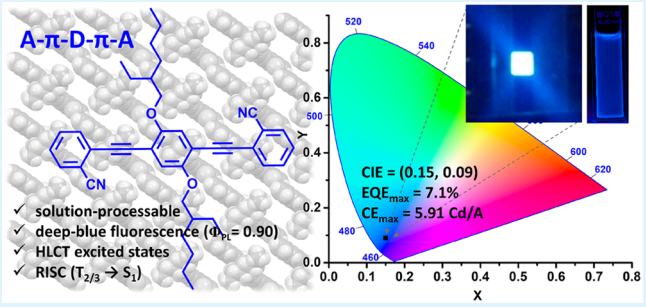

KEYWORDS: *deep-blue OLED, electroluminescence, fluorescent small molecule, oligo(p-phenyleneethynylene), hybridized local and charge transfer (HLCT) state, reverse intersystem crossing (RISC), hot-exciton*

INTRODUCTION

The development of solution-processable fluorescent small molecules with deep-blue electroluminescence (EL) characteristics is at the forefront of organic light-emitting diode (OLED) research for high-resolution full-color displays and solid-state lightings.[1−4] Designing and synthesizing new molecular systems with highly efficient deep-blue emission are very important not only to widen the color gamut and reduce power consumption in full-color displays but also to excite lower energy emissive sources to generate other color coordinates and white lighting via energy cascade.[5,6] As compared to polymer-based materials,[7,8] small molecules typically offer unique benefits in terms of ease of synthesis/purification, ultrahigh material purity, monodispersity with well-defined chemical structure, good solubility in common solvents, and synthetic reproducibility (*minimum batch-to-batch variation*).[9−17] These advantages make fluorescent small molecules a very attractive class of emissive material for the

Received: July 23, 2019
Accepted: October 14, 2019
Published: October 14, 2019

DOI: 10.1021/acsami.9b12971
ACS Appl. Mater. Interfaces 2019, 11, 44474−44486

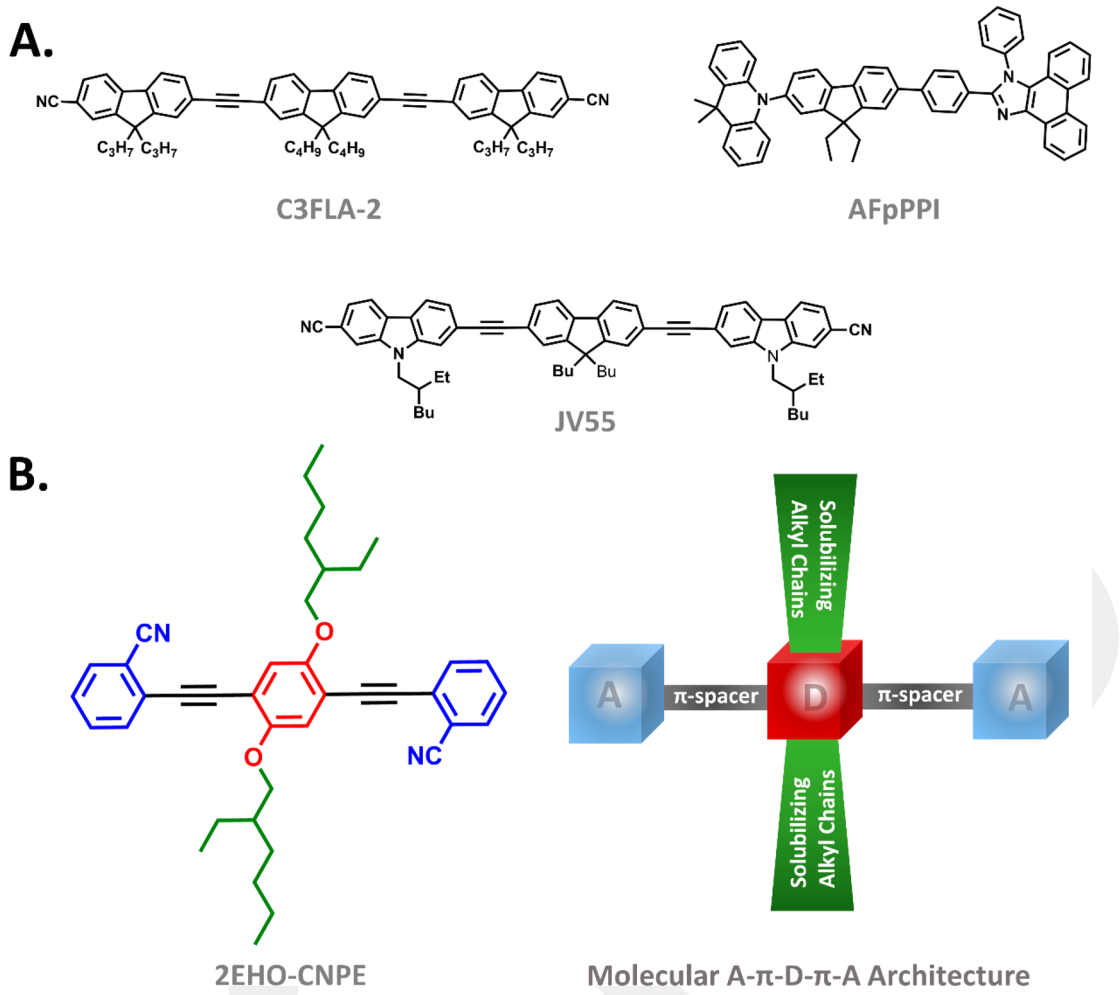

Figure 1. (A) Chemical structures of solution-processable deep-blue fluorescent small molecules reported in the literature with values of EQE_{max} > 5% in the OLEDs.[27,31,33] (B) The chemical structure of 2EHO−CNPE developed in this study showing the corresponding donor (D), acceptor (A), π-spacer, and solubilizing units.

development of OLED applications, especially for the fabrication of cost-effective large-area display or lighting devices via roll-to-roll processes such as inkjet printing (*noncontact patterning*).[18−24] Since the demonstration of the first electroluminescent device exploiting the fluorescent metal−chelate complex tris(8-hydroxyquinolinato)aluminum (Alq_3) more than 3 decades ago,[25] a wide range of molecular π-structures has been developed and studied to yield high-performance OLEDs with varied color coordinates.[26] Among these, however, deep-blue emitting small molecules are still scarce as far as color purity, device performance, and solution-processability are concerned. The design of new molecular architectures showing good solution processability, wide optical band gap (≥2.9 eV), deep-blue emission with Commission Internationale de l'Eclairage (CIE) (x, y) coordinates of (0.14, 0.08) as defined by the National Television System Committee (NTSC), energetically/spatially favorable frontier molecular orbitals, and good charge-transport/electroluminescence remains to be very challenging. To realize all of these properties in a single molecular system requires rationally engineered π-structures. Until today, a limited number of molecular systems employing fused/heterocyclic aromatic π-units such as fluorene,[27,28] naphthalene/anthracene,[29,30] carbazole,[1,31,32] phenanthroimidazole,[33] and triarylamine[34] have simultaneously achieved all of these properties to yield deep-blue emission in OLEDs (Supporting Information Table S1). And, among these structures, only a few of them could exhibit maximum external quantum efficiencies (EQE_{max}s) greater than 5%.[27,31,33,34] (Table S1) It is noteworthy that, despite some intrinsic photophysical limitations such as the presence of a nonradiative pathway via metal d-orbitals and donor−acceptor configurations causing intramolecular charge transfer transitions,[19,35−38] phosphorescent and thermally activated delayed fluorescence (TADF) emitters have also demonstrated great promise in deep-blue OLEDs upon rational materials design.[39−45] However, the majority of these compounds have been processed into their emissive thin films via physical vapor deposition (*thermal evaporation*). Only recently, solution-processed films of sulfone-based and adamantyl based deep-blue TADF emitters are reported with EQE_{max}s over 5−6% in OLEDs.[36,46] Therefore, from a materials design and development perspective, realizing highly efficient deep-blue fluorescence based on solution-processed novel π-architectures is very important both to advance the existing device performances and to diversify the material properties in deep-blue OLEDs.

To this end, rod-shaped oligo(*p*-phenyleneethynylene)s have yet to be explored in deep-blue emissive OLEDs despite some earlier theoretical and experimental studies pointing out their promising photophysical and charge-transport character-

DOI: 10.1021/acsami.9b12971
ACS Appl. Mater. Interfaces 2019, 11, 44474−44486

istics.[47] There are only a few examples of OLED devices fabricated with an oligo(*p*-phenyleneethynylene)-based emissive layer, and they typically emit in the blue/green spectral region with low EQE_{max}s of ∼0.5−2.4%.[48−50] Specifically, earlier reports revealed that when these π-systems are functionalized with donor (D) and/or acceptor (A) substituents, they could achieve tunable fluorescence emission with high solution/solid-state quantum yields.[51−55] These earlier findings with promising optoelectronic/photophysical characteristics have prompted us to develop and study a novel donor/acceptor functionalized oligo(*p*-phenyleneethynylene) molecule for highly efficient deep-blue OLEDs.

In this report, we demonstrate the theory-aided molecular design, synthesis, and full characterization of a new oligo(*p*-phenyleneethynylene) molecule 1,4-bis((2-cyanophenyl)-ethynyl)-2,5-bis(2-ethylhexyloxy)benzene (2EHO−CNPE) (Figure 1). The new molecular backbone has a rod-shaped π-conjugated system employing 2-cyanophenyl acceptor (A) end units linked to a central bis(2-ethylhexyloxy)benzene donor (D) via ethynylene π-spacers to form an A−π−D−π−A molecular architecture. The single-crystal structure and thermal, photophysical, and electrochemical properties as well as the electroluminescence devices of the new molecule have been studied. High-photoluminescence quantum efficiencies (Φ_{PL}s) of 0.90 and 0.51 were measured in chloroform solution and as thin film in CBP host, respectively, by using an integrating sphere method. OLEDs with a device architecture of ITO/PEDOT:PSS/CBP:2EHO−CNPE/TPBI/Ca/Al, in which the emissive layer is solution-processed, showed excellent deep-blue electroluminescence (CIE(*x*,*y*) = (0.15, 0.09)) with an impressive maximum external quantum efficiency of 7.06% (EQE = 6.30% at 200 cd/m^2) and a maximum current efficiency of 5.91 cd/A (CE = 5.34 cd/A at 200 cd/m^2). In addition to showing the first time deep-blue electroluminescence of an oligo(*p*-phenyleneethynylene) derivative, the device performance shown here is among the highest achieved to date for a deep-blue OLED based on a solution-processed fluorescent molecule. TDDFT calculations indicate that the observed high radiative exciton yield (η_r ∼ 69%) originates from reverse intersystem crossing (RISC) between the high-lying triplet states and the first singlet excited state ($T_2/T_3 \rightarrow S_1$), all having hybridized local and charge transfer (HLCT) excited state characteristics.

EXPERIMENTAL SECTION

Materials and Methods. In the reactions, conventional Schlenk techniques were used, and the reactions were performed under N_2 unless otherwise noted. All reagents were obtained from commercial sources and used without any purification unless otherwise noted. $^1H/^{13}C$ NMR characterizations were performed on a Bruker 400 spectrometer (^1H, 400 MHz; ^{13}C, 100 MHz). Elemental analyses were performed on a LecoTruspec Micro model instrument. MALDI-TOF was performed on a Bruker Microflex LT MALDI-TOF-MS instrument. Thermogravimetric analysis (TGA) and differential scanning calorimetry (DSC) measurements were performed on Mettler Toledo-TGA/STDA 851 and Mettler Toledo-DSC 822 model instruments, respectively, at a heating rate of 10 °C/min under nitrogen. UV−vis absorption and photoluminescence emission measurements were recorded on a Shimadzu, UV-1800 UV−vis spectrophotometer and a Fluoracle FS5 spectrofluorometer (Edinburgh Instruments), respectively. The PL quantum yields in solution and solid state were measured (λ_{exc} = 350 nm) by an absolute method (calibrated integrating sphere) using a Hamamatsu absolute PL quantum yield spectrometer C11347. Electrochemistry was performed on a C3 cell stand electrochemical station equipped with BAS-Epsilon software (Bioanalytical Systems, Inc. Lafayette, IN, USA). All theoretical calculations were carried out using density functional theory (DFT) and time-dependent density functional theory (TDDFT) at the B3LYP/6-311G** level by using Gaussian 09.[56]

Synthesis and Structural Characterization. *Synthesis of 1,4-Dibromo-2,5-bis(2-ethylhexyloxy)benzene (**1**).* To a mixture of potassium carbonate (1.545 g, 11.18 mmol) and 2-ethylhexyl bromide (3.03 g, 15.69 mmol) dissolved in 15 mL of DMF, 2,5-dibromohydroquinone (1.55 g, 5.78 mmol) was slowly added under nitrogen. The resulting reaction solution was stirred at 100 °C for 48 h. The mixture was then cooled to room temperature and quenched with water. The reaction mixture was extracted with dichloromethane, and the organic phase was washed with water, dried over Na_2SO_4, filtered, and evaporated to dryness to give the crude product. The crude was then purified by column chromatography on silica gel using hexane as the eluent to give compound **1** as a colorless oil (2.51 g, 88% yield). ^1H NMR (400 MHz, $CDCl_3$): δ 7.09 (s, 2H), 3.84 (d, 4H, *J* = 4.0 Hz), 1.74−1.77 (m, 2H), 1.43−1.57 (m, 8H), 1.32−1.35 (m, 8H), 0.91−0.96 (m, 12H).

*Synthesis of 1,4-Bis(ethynyltrimethylsilane)-2,5-bis(2-ethylhexyloxy)benzene (**2**).* A mixture of 1,4-dibromo-2,5-bis(2-ethylhexyloxy)benzene (**1**; 2.5 g, 5.08 mmol), $Pd(PPh_3)_2Cl_2$ (0.214 g, 0.305 mmol), and CuI (0.049 g, 0.254 mmol) in Et_3N (50 mL) was stirred for 10 min. Ethynyltrimethylsilane (1.247 g, 12.7 mmol) was then added, and the reaction mixture was heated at 90 °C under nitrogen for 48 h. Then, the reaction mixture was cooled to room temperature and filtered; the filtrate was evaporated to dryness to yield a crude mixture, which was then purified by column chromatography on silica gel using hexane:ethyl acetate (30:1) eluent to yield **2** as a yellow oil (1.56 g, 58% yield). ^1H NMR (400 MHz, $CDCl_3$): δ 6.89 (s, 2H), 3.82−3.87 (m, 4H), 1.72−1.75 (m, 2H), 1.44−1.58 (m, 8H), 1.32−1.34 (m, 8H), 0.91−0.96 (m, 12H), 0.26 (s, 18H).

*Synthesis of 1,4-Bis(ethynyl)-2,5-bis(2-ethylhexyloxy)benzene (**3**).* The suspension of 1,4-bis(ethynyltrimethylsilane)-2,5-bis(2-ethylhexyloxy)benzene (**2**; 1.56 g, 2.96 mmol) and KOH (4.99 g, 88.95 mmol) in THF:methanol (9:1; 150 mL) was stirred at room temperature for 1 h. Next, the reaction mixture was quenched with water, and the resulting solution was extracted with dichloromethane. The organic phase was washed with water, dried over Na_2SO_4, filtered, and evaporated to dryness to yield **3** as a yellow oil (1.07 g, 94.5% yield). ^1H NMR (400 MHz, $CDCl_3$): δ 6.96 (s, 2H), 3.85 (d, 4H, *J* = 4.0 Hz), 3.32 (s, 2H), 1.75−1.78 (m, 2H), 1.46−1.57 (m, 8H), 1.27−1.34 (m, 8H), 0.91−0.96 (m, 12H).

Synthesis of 1,4-Bis((2-cyanophenyl)ethynyl)-2,5-bis(2-ethylhexyloxy)benzene (2EHO−CNPE). The reagents 2-iodobenzonitrile (0.554 g, 2.42 mmol), CuI (0.009 g, 0.048 mmol), and $Pd(PPh_3)_2Cl_2$ (0.068 g 0.097 mmol) in Et_3N:THF (2:1; 30 mL) were stirred for 5 min. Then, 1,4-bis(ethynyl)-2,5-bis(2-ethylhexyloxy)-benzene (**3**; 0.37 g, 0.97 mmol) in 5 mL of THF was added, and the resulting reaction mixture was heated at 80 °C under nitrogen for 24 h. Then, the solution was cooled to room temperature and evaporated to dryness. The crude was then purified by column chromatography on silica gel using hexane:ethyl acetate (3:1) as the eluent to give the pure 2EHO−CNPE as a light yellow solid (0.283 g, 50%). ^1H NMR (400 MHz, $CDCl_3$): δ 7.69 (d, 2H, *J* = 8.0 Hz), 7.62 (d, 2H, *J* = 8.0 Hz), 7.56−7.60 (m, 2H), 7.40−7.45 (m, 2H), 7.10 (s, 2H), 3.94−3.96 (m, 4H), 1.82−1.85 (m, 2H), 1.54−1.57 (m, 8H), 1.32−1.37 (m, 8H), 0.97 (t, 6H, *J* = 8.0 Hz), 0.88 (t, 6H, *J* = 8.0 Hz). ^{13}C NMR (100 MHz, $CDCl_3$): δ 154.1, 132.7, 132.4, 132.3, 128.2, 127.4, 117.6, 116.8, 114.9, 113.7, 92.6, 91.0, 72.0, 39.5, 30.6, 29.1, 24.0, 23.1, 14.1, 11.2. mp = 116−117 °C. MS(MALDI-TOF) *m*/*z* (M^+). Calcd for $C_{40}H_{44}N_2O_2$: 584.34. Found: 584.951 for $[M]^+$, 471.566 for $[M - 2EH]^+$, 359.359 for $[M - 2(2EH)]^+$. Anal. Calcd for $C_{40}H_{44}N_2O_2$: C, 82.15; H, 7.58; N, 4.79. Found: C, 82.48; H, 7.73; N, 4.70.

Device Fabrication and Characterization. The light-emitting diode device structure is ITO/PEDOT:PSS/CBP:2EHO−CNPE/TPBI/Ca/Al. The patterned indium tin oxide (ITO)-coated (120 nm) glass (Kintec Co.) with a sheet resistance of 10 Ω sq^{-1} was used as the substrate. The substrates were cleaned with detergent PCC-54

DOI: 10.1021/acsami.9b12971
ACS Appl. Mater. Interfaces 2019, 11, 44474−44486

Scheme 1. Synthesis of Deep-Blue Emissive Molecule 1,4-Bis((2-cyanophenyl)ethynyl)-2,5-bis(2-ethylhexyloxy)benzene (2EHO−CNPE)

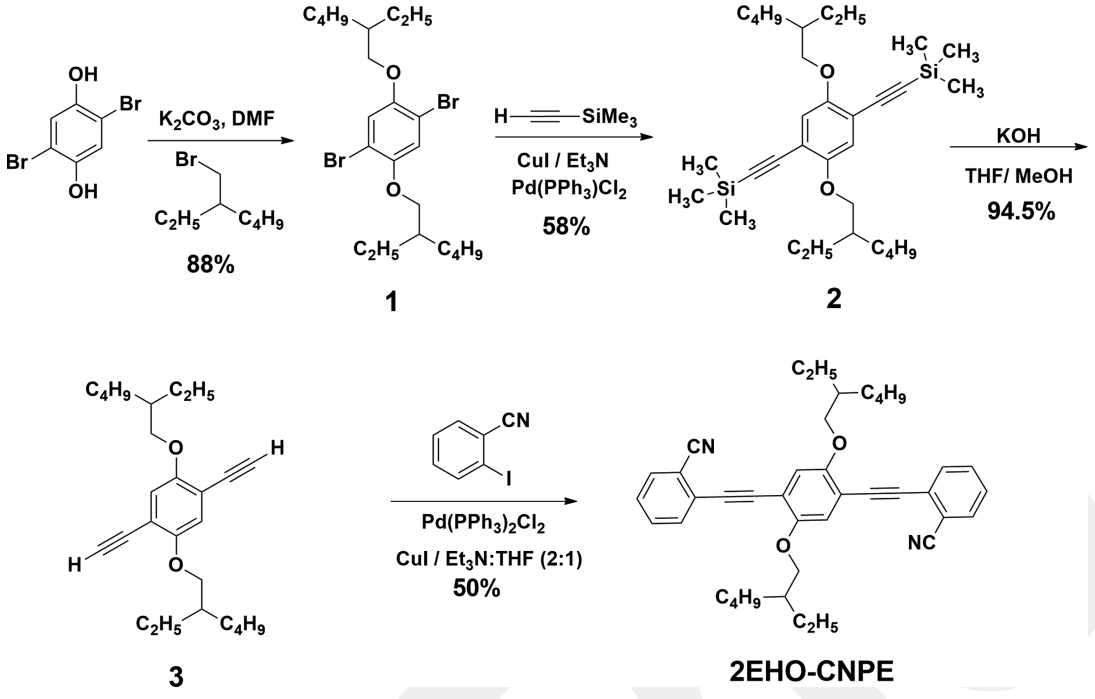

solution (2 wt % dispersed in H_2O), distilled water, acetone, ethanol, and isopropanol in an ultrasonic solvent bath and treated by oxygen plasma for 5 min. Poly(3,4ethylenedioxythiophene):poly-(styrenesulfonate) (PEDOT:PSS, Heraeus Clevios GmbH) was spin-coated (3000 rpm for 60 s) on ITO-glass substrates as the hole injection layer (60 nm) and baked at 120 °C for 20 min. Next, the emissive layer was spin-coated (800 rpm for 40 s) from a solution of 0.4 mg of 2EHO−CNPE and 9.6 mg of CBP (2EHO−CNPE mole fraction = 3.4%) in 1 mL of chloroform, which was annealed at 70 °C for 10 min to remove residual solvent. Note that this mole fraction was chosen as the optimum number to yield the best device performance after trying a number of different ratios. The thickness of the emissive layer was measured as 55 nm. In equivalent devices, the emissive layer consisting of neat 2EHO−CNPE film (50 nm) was prepared by spin-coating (800 rpm for 40 s) 2EHO−CNPE solution in chloroform (8.0 mg/mL) and annealing at 70 °C for 10 min to remove residual solvent. Finally, an electron-transporting/hole-blocking layer of 1,3,5-tris(phenyl-2-benzimidazolyl)benzene (TPBI, 40 nm) and a cathode composed of calcium (10 nm) and aluminum (100 nm) were sequentially deposited via thermal evaporation under high vacuum (2×10^{-6} mBar). The size of the active OLED area is 9 mm^2 as defined by shadow masks. The electroluminescence spectra and current density−voltage−brightness of the devices were measured with a Hamamatsu PMA-12 C10027 photonic multichannel analyzer and digital multimeter (2427-C 3A Keithley). All of the measurements were carried out at room temperature under ambient conditions. A stylus profiler (KLA Tencor P-6) was used to measure the thickness of the organic layers. The surface morphology of the emissive CBP:2EHO−CNPE thin film spin-coated on ITO/PEDOT:PSS was characterized by atomic force microscopy (FlexAFM-NanoSurf, Abdullah Gül University-Central Research Facility (AGU-CRF)).

RESULTS AND DISCUSSION

Molecular Design, Synthesis, and Characterization. In the molecular structure of 2EHO−CNPE, the terminal phenyl rings are functionalized with cyano (-CN) electron-withdrawing substituents and the central phenyl ring is functionalized with 2-ethylhexyloxy (-$OCH_2CH(C_2H_5)C_4H_9$) electron-donating substituents. Instead of forming direct D−A bonds, ethynylene is used as a proper π-conjugation spacer group in an A−π−D−π−A molecular architecture. This design is envisioned to enable a wide optical band gap and facilitate efficient fluorescence emission in the high-energy spectral region by governing the formation of local (LE) and charge-transfer (CT) excited states. The simultaneous utilization of LE and CT characteristics by forming a hybridized local and charge-transfer excited state (HLCT) would allow for both high quantum efficiency ($\Phi_{PL} \rightarrow 1.0$) and a large fraction of singlet exciton generation (radiative exciton yield (η_r) $\gg$ 25%) during electroluminescence.[57,58] Also, the presence of both donor and acceptor π-moieties in the same molecular structure could yield ambipolar charge transport (i.e., concurrent conduction of electrons and holes) to benefit the EL performance in OLEDs.[59] Finally, 2-ethylhexyloxy (-$OCH_2CH(C_2H_5)C_4H_9$) substituents provide good solubility for efficient synthesis/purification and emissive film fabrication. The presence of swallow-tailed bulky substituents at the central unit in a relatively small-sized molecular dimension is expected to impede undesired π−π interactions in the solid state that could otherwise yield excimer formation (*red shift in emission*) and induce nonradiative decay pathways (*low quantum yield*). The quantum mechanical modeling (DFT, B3LYP/6-311G**) performed on 2EHO−CNPE prior to the synthesis shows the presence of delocalized HOMO and LUMO frontier molecular orbitals (Figure S1). While the LUMO delocalizes along the entire molecular π-system, HOMO tends to delocalize on the dialkyloxyphenyl and ethynylene units with minimal contributions from the cyanophenyl end units. Therefore, it is very likely that both LE and CT characteristics would be utilized during electronic transitions. The theoretical HOMO and LUMO energies are found to be −5.61 eV and −2.46 eV, respectively, and the calculated absorption spectra indicate that $S_0 \rightarrow S_1$ (HOMO → LUMO; f = 1.03) electronic transition occurs at an energy

DOI: 10.1021/acsami.9b12971
ACS Appl. Mater. Interfaces 2019, 11, 44474−44486

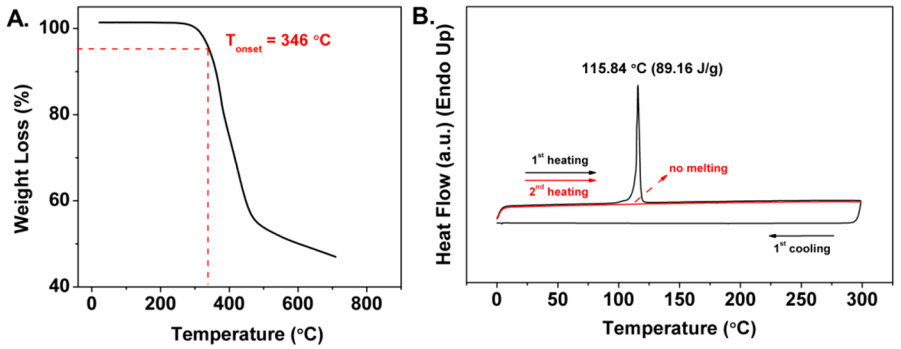

Figure 2. (A) Thermogravimetric analysis (TGA) and (B) differential scanning calorimetry measurement curves of 2EHO−CNPE at a temperature ramp of 10 °C/min under N_2.

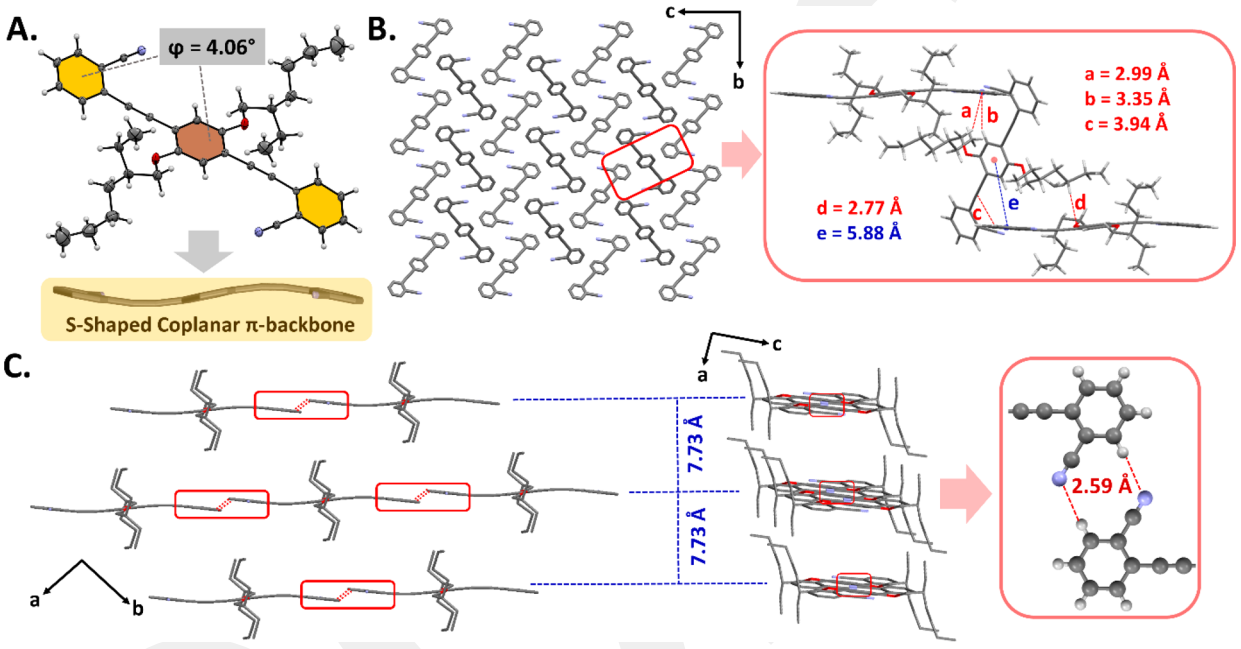

Figure 3. (A) ORTEP drawing of the molecular structure for 2EHO−CNPE (20% probability level) showing the corresponding torsion angles and π-backbone coplanarity. (B) Perspective views of the herringbone arrangements viewed along the crystallographic *a*-axis showing "C−H···π" interactions (a = 2.99 Å, b = 3.35 Å, c = 3.94 Å, and d = 2.77 Å) and centroid-to-centroid distance (e = 5.88 Å). The flexible alkyl side chains are omitted for clarity. (C) Perspective view of the layered network showing strong intermolecular "-CH···N" (2.59 Å) hydrogen bonding interactions within the layers and large interlayer centroid-to-centroid distances (7.73 Å).

value of 2.85 eV (Figure S1). These initial theoretical results, as the first guess, indicate that the new molecule could yield an efficient deep-blue electroluminescence with favorable emission characteristics and charge injection/transport from conventional electron/hole-injection/transport layers. We also note that these results are found to be in good agreement with the experimental observations (vide infra).

As depicted in Scheme 1, the synthesis of 2EHO−CNPE was carried out by successive Sonogashira cross-coupling reactions. 2,5-Dibromohydroquinone was first reacted with 2-ethylhexyl bromide in DMF in the presence of K_2CO_3 base to give **1** in 88% yield. Then, **1** underwent a double Sonogashira cross-coupling reaction with ethynyltrimethylsilane (HC≡C−$SiMe_3$) in the presence of $Pd(PPh_3)_2Cl_2$ catalyst and CuI/Et_3N co-catalyst/base mixture. Trimethylsilyl substituted compound **2** was obtained in 58% yield, which was then quantitatively (94.5% yield) desilylated in the presence of a strong base (KOH) in a THF/methanol mixture to afford hydrogen-ended ethynyl groups in **3**. In the final Sonogashira cross-coupling step, **3** was double reacted with the acceptor unit 2-iodobenzonitrile in the presence of $Pd(PPh_3)_2Cl_2$ catalyst and CuI/Et_3N co-catalyst/base mixture, which yielded the final compound 2EHO−CNPE in 50% yield after chromatographic purification. The well-defined structures and chemical purities of the intermediate compounds and the final small molecule were adequately verified by $^1H/^{13}C$ NMR spectroscopies (Figures S2−S6, Supporting Information), MALDI-TOF mass spectrometry (Figure S7, Supporting Information), and elemental analysis.

Thermal Properties. Thermogravimetric analysis indicated high thermal stability for 2EHO−CNPE with the thermolysis onset temperature (corresponding to 5% weight loss) of 346 °C (Figure 2A). The thermal transitions of 2EHO−CNPE were studied via differential scanning calorimetry (DSC) measurements (Figure 2B), which showed a sharp endothermic peak (enthalpy of +89.16 J/g) at 115.84 °C without any corresponding crystallization peak. The endothermic peak is assigned to a crystal to isotropic-liquid transition

DOI: 10.1021/acsami.9b12971
ACS Appl. Mater. Interfaces 2019, 11, 44474−44486

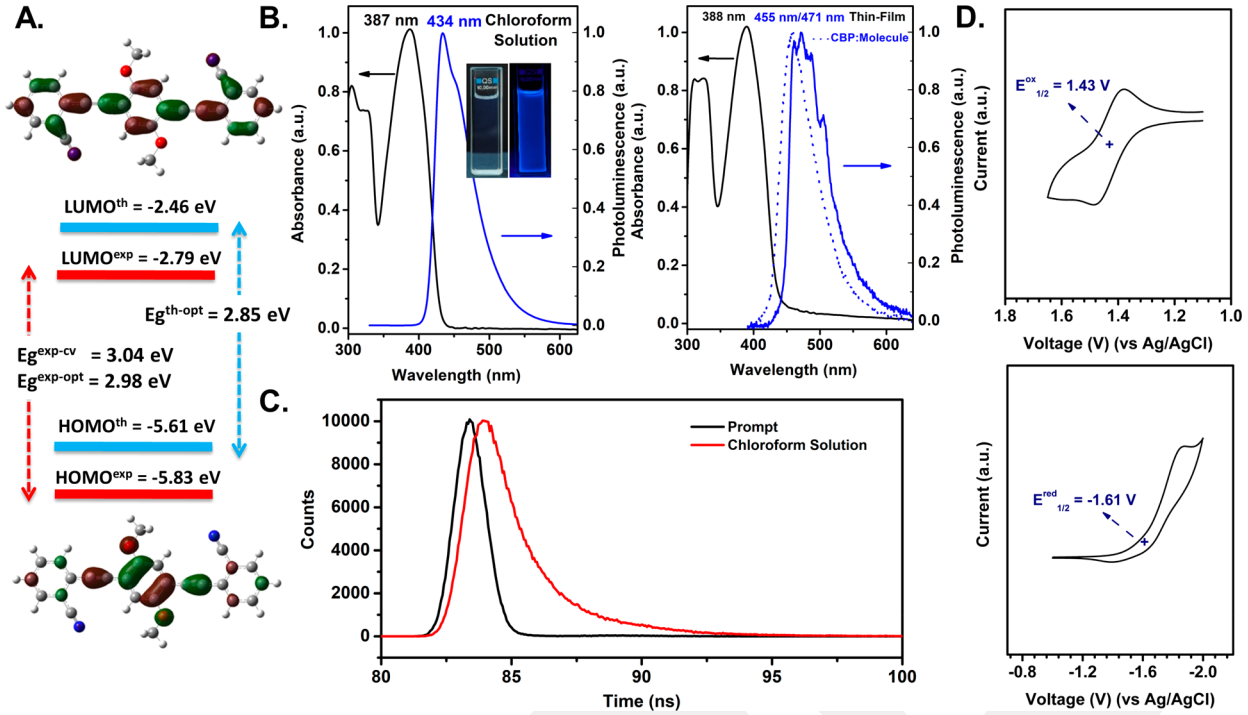

Figure 4. (A) Energy diagram showing theoretically calculated (blue) and experimentally estimated (red) HOMO/LUMO energy levels of 2EHO−CNPE as well as their topographical representations (B3LYP/6-311G** level of theory). (B) Optical absorption (black line) and photoluminescence (blue line) spectra of 2EHO−CNPE in chloroform (1.0×10^{-5} M), and as spin-coated neat and CBP-doped (4.0 wt % 2EHO−CNPE) thin films on glass. Inset: Optical images of 2EHO−CNPE solution in chloroform under room light and optical excitation. (C) Transient photoluminescence decay profile measured at 430 nm for 2EHO−CNPE solution (10^{-5} M) in chloroform upon excitation at 390 nm. (D) Cyclic voltammograms of 2EHO−CNPE showing oxidation and reduction peaks in 0.1 M $TBAPF_6/CHCl_3$ solution vs Ag/AgCl (3.0 M NaCl) at a scan rate of 100 mV/s.

since it correlates well with the melting temperature ($T_{m.p.}$ = 116−117 °C) measured by conventional melting point apparatus. The absence of exothermic peak during cooling indicates that the isotropic liquid of 2EHO−CNPE does not crystallize back to a crystalline phase, rather forms an amorphous solid. This was confirmed by the successive heating experiment performed on this heated−cooled solid, which did not show a melting peak again. Despite the presence of two highly flexible, swallow-tailed 2-ethylhexyloxy substituents at the central benzene ring, high thermal stability and reasonably good melting temperature of 2EHO−CNPE can be attributed to π-rigidity of the rod-shaped acceptor−π−donor−π−acceptor molecular structure. The good solubility in common organic solvents along with the observed thermal characteristics should enable solution-based fabrication of 2EHO−CNPE films with the required thermal processing that is typically performed at temperatures below 80 °C in OLEDs.

Single-Crystal Structure and Intermolecular Interactions. The solid-state characteristics of 2EHO−CNPE were studied by single-crystal X-ray analysis in order to gain more insight into the molecular structure, packing, and intermolecular interactions with regard to structure−property relationships of photo-/electroluminescent materials. Clear yellow needle-like crystals of 2EHO−CNPE suitable for X-ray diffraction were obtained by slow evaporation of chloroform/hexane mixture (1:1). The molecule adopts an S-shaped nearly coplanar π-conjugated molecular framework (Figure 3A) that crystallizes in the *C*2/*c* space group (*monoclinic*) in a herringbone pattern (Figure 3B). In the molecular structure, cyanophenyl end units are found to employ an antiparallel arrangement with respect to each other providing a molecular inversion center, and a small dihedral angle of 4.06° was measured between cyanophenyl end units and the central dialkyloxyphenyl unit. This matches well with the coplanar conformations of previously reported functionalized phenyleneethynylenes[54,60] and indicates that the π-conjugation could extend over the complete molecular system. Strong intermolecular "C−H···N (2.59 Å)" hydrogen bonding interactions are present (Figure 3C) between cyanophenyl end units of the neighboring 2EHO−CNPE molecules. Each molecule is found to be involved in four hydrogen bonding interactions from both cyanophenyl end units, which helps the extension of a one-dimensional slipped stacked π-network. Note that the electropositive hydrogens (H3) involved in these interactions are in *ortho*-positions to the electron withdrawing cyano substituents, which enables the formation of hydrogen-bonded dimers at each end (Figure 3C, inset). Despite the molecular coplanarity and the extension of a one-dimensional π-network, the presence of flexible $-OCH_2CH(C_2H_5)C_4H_9$ chains on the central benzene ring was found to prevent efficient cofacial $\pi-\pi$ interactions (centroid-to-centroid distance = 7.73 Å). This is very consistent with our original design rationales to avoid $\pi-\pi$ interactions for efficient deep-blue emission. On the other hand, centroid-to-centroid distances of 5.88 Å were measured between dialkyloxybenzene and cyanophenyl rings for the neighboring tilted molecules in the herringbone-like orientation (Figure 3B), which is considered to be too large for an effective $\pi-\pi$ interaction. In this arrangement, also "C−H···π" interactions with distances of 2.99 Å/3.35 Å were identified between the cyanophenyl rings and the aliphatic/

DOI: 10.1021/acsami.9b12971
ACS Appl. Mater. Interfaces 2019, 11, 44474−44486

aromatic hydrogens of the central dialkyloxyphenyl ring (Figure 3B). The shortest C−H···π interaction was observed at a distance of 2.68 and 2.77 Å between the aliphatic hydrogens of the hexyl chain (H20) and the cyanophenyl and dialkyloxybenzene rings, respectively. On the other hand, relatively weaker C−H···π (3.94 Å) interactions were found between cyanophenyl aromatic hydrogens and the ethynylene units. All of these interactions are found to play key roles in the solid-state packing of 2EHO−CNPE to generate a herringbone pattern with limited π-interactions and no specific $\pi-\pi$ interactions. Similar herringbone crystal packings via C−H···π interactions were previously observed in alkyloxy substituted similar sized phenyleneethynylenes.[54]

Photophysical and Electrochemical Properties. The optical absorption and fluorescence properties of 2EHO−CNPE are evaluated by UV−vis absorption and photoluminescence spectroscopies both in chloroform solution (1.0×10^{-5} M) and as thin films (Figure 4). In solution, the absorption maximum (λ_{max}) is observed at 387 nm corresponding to $\pi-\pi^*$ ($S_0 \rightarrow S_1$) transition of the cyano-/alkyloxy-functionalized oligo(*p*-phenyleneethynylene) backbone. The corresponding fluorescence spectrum shows a sharp emission peak with a maximum at 434 nm and a relatively narrow full width at half-maximum (fwhm) of 52 nm. The Commission International de L'Eclairage (CIE) color coordinates of (0.15, 0.09) are measured, which correspond to the deep-blue spectral region. High-photoluminescence quantum efficiency (Φ_{PL}) of 0.90 was determined in chloroform solution by using an integrating sphere method. Note that the optical absorption/fluorescence spectra of the nonfunctionalized parent oligo(*p*-phenyleneethynylene) π-system (Figure S8) were previously reported to be in the UV spectral region (λ_{abs} = 328 nm; λ_{em} = 348 nm).[52,53] Thus, the observed deep-blue fluorescence for 2EHO−CNPE is undoubtedly the result of rational donor (2EHO−)/acceptor-(−CN) functionalization on the oligo(*p*-phenyleneethynylene) π-system. The optical band gap is calculated as 2.98 eV from the intersection of low-energy absorption ($\lambda_{abs(0-0)}$) and high-energy emission ($\lambda_{em(0-0)}$) spectral band edges, which correlates perfectly with the theoretical $S_0 \rightarrow S_1$ electronic transition (2.85 eV) estimated by the TDDFT calculation. As shown in Figure S9, upon increasing solvent polarity (toluene (ε = 2.38) → chloroform (ε = 4.81) → THF (ε = 7.52) → dichloromethane (ε = 9.08) → ethanol (ε = 24.6)),[61,62] although the absorption spectra barely change, the emission spectra exhibit positive solvatochromism (λ_{em} = 432 nm (toluene) → 440 nm (ethanol)) along with slight band broadening ($\Delta\lambda_{fwhm} \sim$ 5 nm) and disappearance of the vibronic structure. This indicates that radiative local excited state has some contribution from a charge-transfer moiety. The excited-state properties were further investigated by studying transient photoluminescence decay profile in solution (10^{-5} M in chloroform) at 430 nm (λ_{exc} = 390 nm), which showed a single-exponential decay with a short lifetime of 2.32 ns; no delayed component was observed (Figure 4C).

In view of all of these findings (i.e., high quantum yield, one lifetime decay profile with no delayed component, and positive solvatochromism in fluorescence), the emission seems to originate from the prompt decay of the S_1 state that has a hybridized local and charge-transfer character. This HLCT state formation agrees well with the calculated natural transition orbitals (NTOs) and excited-state properties (vide infra), and it is clearly the result of our current molecular design employing ethynylene π-spacers between dialkyloxybenzene (D) and cyanophenyl (A) units forming large frontier orbitals' overlap across the molecular system (*large transition moment*) with controlled spatial separation.[57,63] In addition, the coplanar structure of the new molecule is very likely to avoid the formation of pure charge-transfer states via intramolecular twists that would deteriorate the fluorescence quantum yield. The formation of HLCT excited states has been demonstrated as an important approach for the design of donor−acceptor fluorescent small molecules that can achieve a combination of high fluorescence quantum yield ($\Phi_{PL} \rightarrow 1$) and large radiative exciton yield ($\eta_r \gg 25\%$) in electroluminescence by using $T_{(n>1)} \rightarrow S_1$ reverse intersystem crossings.[57,58] Going from dilute solution to solid state (neat thin film), although the absorption profile exhibited insignificant change, the emission profile of the neat 2EHO−CNPE film showed a red shift of ∼37 nm (λ_{em} = 434 → 471 nm) along with a spectral broadening ($\Delta\lambda_{fwhm} \sim$ 15−20 nm) and vibronic-structure formation (Figure 4B). Despite the absence of strong $\pi-\pi$ interactions in the solid state, this moderate spectral shift likely indicates the formation of weakly bound excimer (*energetically stabilized* S_1) via intermolecular C−H···N/π interactions as identified in the single-crystal structure (vide supra). Note that the presence of these intermolecular interactions does not affect the ground state (S_0) of 2EHO−CNPE since the absorption profile remains the same going from solution to solid state. Solid-state Φ_{PL} in thin-film phase was determined as 0.41 using integrating-sphere method. As a result of red-shifted emission spectrum, CIE color coordinate for the neat thin-film emission is found to deviate from the deep-blue region. However, when 2EHO−CNPE (4.0 wt %) was doped into a 4,4′-bis(*N*-carbazolyl)-1,1′-biphenyl (CBP; 96.0 wt %) host, the photoluminescence profile was found to be blue-shifted (λ_{em} = 471 → 455 nm) as compared to the neat thin film yielding again deep-blue emission with increased photoluminescence quantum efficiency of Φ_{PL} = 0.51. The absence of the emission peak from the host material CBP (Figure S10, $\lambda_{em} \sim$ 388 nm for $\lambda_{exc.}$ = 355 nm) indicates very efficient host-to-guest energy- or charge-transfer processes. Since there is a strong spectral overlap between the emission band of the CBP host and the absorption band of the 2EHO−CNPE guest, the energy-transfer route is very likely to occur in the current CBP:2EHO−CNPE host:guest system to confine the radiative excitons on 2EHO−CNPE molecules. It is noteworthy that although our original molecular design approach is very effective in eliminating close $\pi-\pi$ stackings (vide supra), solid-state interactions of other types (e.g., C−H···N/π) clearly cause the emission to somewhat deviate from the deep-blue spectral region. Therefore, the 2EHO−CNPE-based emissive layer in the electroluminescent device is fabricated with an energetically suitable host (i.e., CBP) to fully avoid aggregation-induced emission characteristics.

The frontier molecular orbital energies and electrochemical properties of 2EHO−CNPE were characterized by cyclic voltammetry in solution. As shown in Figure 4D, clear (quasi)reversible oxidation and reduction peaks at 1.43 and −1.61 V (vs Ag/AgCl), respectively, were observed indicating bipolar injection characteristics (p-/n-doping) of the current molecule, which should facilitate both hole and electron transport in the emissive layer. The HOMO and LUMO energy levels are estimated to be −5.83 eV and −2.79 eV, respectively, yielding an electrochemical band gap of 3.04 eV, which matches well with the optical band gap and theoretical

DOI: 10.1021/acsami.9b12971
ACS Appl. Mater. Interfaces 2019, 11, 44474−44486

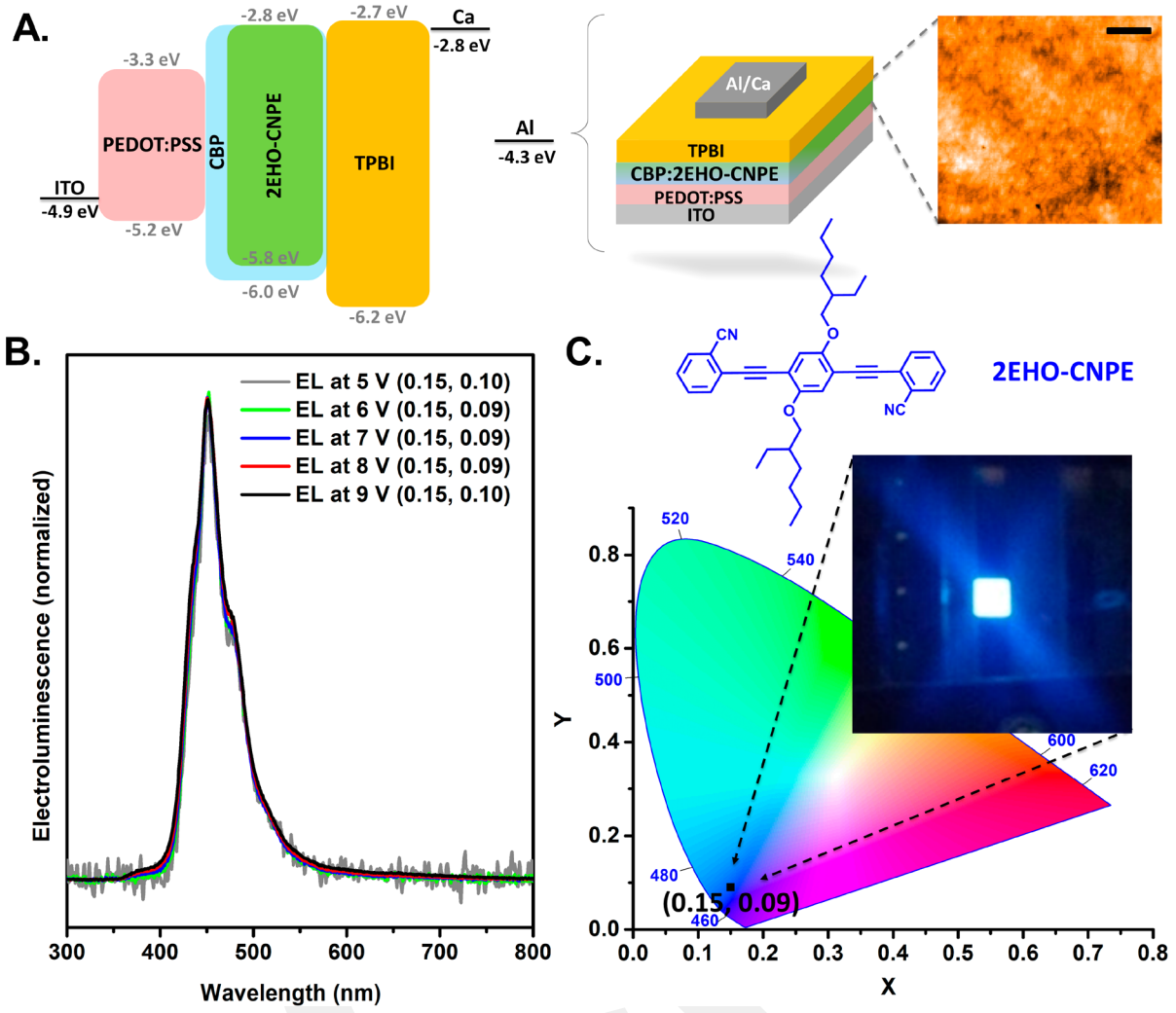

Figure 5. (A) Schematic energy-level diagram and the device architecture for 2EHO−CNPE-based deep-blue emissive OLED (ITO/PEDOT:PSS(60 nm)/CBP:2EHO−CNPE(55 nm)/TPBI(40 nm)/Ca(10 nm)/Al(100 nm)), and the AFM image of spin-coated CBP:2EHO−CNPE (4 wt %) film (~55 nm) on ITO/PEDOT:PSS(60 nm). (The scale bar denotes 1 μm.) (B) EL spectra and corresponding CIE coordinates for OLED devices operated at different voltages. (C) Optical image of the deep-blue emitting OLED device (9 mm^2 active area) during device operation, the chemical structure of 2EHO−CNPE, and CIE 1931 chromaticity diagram showing the deep-blue emission (x,y) coordinates at 200 cd/m^2.

HOMO−LUMO energy gap. As compared to those of various blue-emitting small molecules reported earlier,[6,19,34,59] the relatively stabilized LUMO level of 2EHO−CNPE could be ascribed to the presence of electron withdrawing -CN groups and acetylene units having sp-hybridized carbons. The LUMO level should be favorable for electron injection from electron-transporting layers such as TPBI (LUMO = −2.7 eV) and electron-transport within the emissive layer. Both HOMO and LUMO are found to be fairly delocalized over the entire molecular backbone, which should be advantageous for bipolar charge-transport characteristics.

Electroluminescence Properties. On the basis of its highly efficient deep-blue fluorescence emission and good solubility in common organic solvents, electroluminescence properties of 2EHO−CNPE are studied by fabricating relatively simple OLED devices with a device architecture of ITO/PEDOT:PSS(60 nm)/CBP:2EHO−CNPE(55 nm)/TPBI(40 nm)/Ca(10 nm)/Al(100 nm), in which the emissive layer (CBP:2EHO−CNPE) is prepared by spin-coating chloroform solution of 2EHO−CNPE (4.0 wt %) and CBP (96.0 wt %). As shown in Figure 5A, while PEDOT:PSS serves as hole-injection layer, Ca and TPBI are used as electron-injection and -transporting layers, respectively, based on their favorable energetics with respect to those of 2EHO−CNPE. CBP is used as the host material with good hole-transport characteristics and matching frontier orbital energetics relative to 2EHO−CNPE, which is expected to minimize undesirable intermolecular interactions evident in the neat thin-film fluorescence spectrum of 2EHO−CNPE (vide supra, Figure 4B). The atomic force microscopy (AFM) characterization of the emissive CBP:2EHO−CNPE film spin-coated on ITO/PEDOT:PSS(60 nm) shows the formation of a continuous film morphology with highly interconnected nanosized (~50−100 nm) granular domains and a smooth organic surface with root mean square (RMS) roughness of 0.29−0.35 nm (Figure 5A).

As shown in Figure 5B,C, the device shows an emission with a peak maximum located at 452 nm (at 200 cd/m^2), which corresponds to an excellent deep-blue CIE coordinate of (0.15, 0.09). The electroluminescence spectrum of the OLED device

DOI: 10.1021/acsami.9b12971
ACS Appl. Mater. Interfaces 2019, 11, 44474−44486

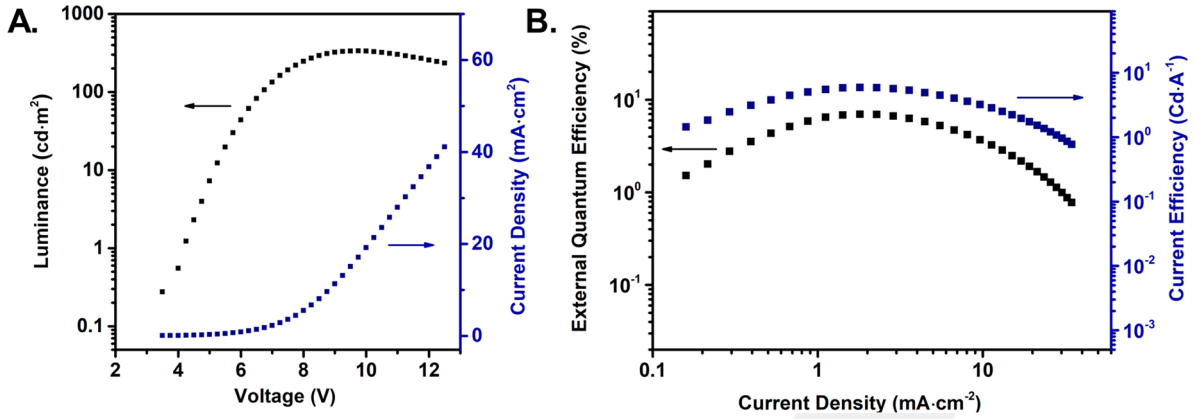

Figure 6. (A) Luminance−voltage and current density−voltage and (B) current efficiency−current density and external quantum efficiency−current density characteristics for the 2EHO−CNPE-based OLED device (ITO/PEDOT:PSS(60 nm)/CBP:2EHO−CNPE(55 nm)/TPBI(40 nm)/Ca(10 nm)/Al(100 nm)).

is identical to the photoluminescence spectra of CBP:2EHO−CNPE (4 wt %) film indicating that the excitons yielding electroluminescence and photoluminescence are essentially the same and the formation of exciplex/excimer is effectively prevented in the current emission layer of CBP:2EHO−CNPE (4 wt %). As shown in Figure S10, the PL spectra for spin-coated thin films of pristine CBP showed an emission peak only at 388 nm with an onset at 430 nm, which indicated that the observed electroluminescence peak at 452 nm originates only from excitons confined on 2EHO−CNPE in the emission layer with no contribution from the CBP host. This indicates the presence of highly favorable charge-/energy-transfer processes from the CBP host matrix to our emissive 2EHO−CNPE molecular system during the electroluminescence process as a result of favorable frontier orbital energetics (Figure 5A). As shown in Figure 5B, the electroluminescence profiles remain the same at various driving voltages from 4 to 9 V with almost no change in the corresponding CIE coordinates. This suggests a voltage-independent, highly stable deep-blue electroluminescence behavior for the current OLED device.

The OLED devices turn-on (1 cd/m^2) at a voltage of 4.1 V, which is as low as the band gap of the emissive small molecule (Figure 6A). A maximum external quantum efficiency of 7.06% (EQE = 6.30% at 200 cd/m^2) and a maximum current efficiency of 5.91 cd/A (CE = 5.34 cd/A at 200 cd/m^2) are recorded for the current 2EHO−CNPE-based OLED device. These performances are among the highest reported to date for a deep-blue OLED based on a solution-processed fluorescent small molecule. Furthermore, to the best of our knowledge, this is the first time that a deep-blue OLED device is reported using an oligo(*p*-phenyleneethynylene) emitter. On the other hand, in order to better understand the electroluminescence characteristics of 2EHO−CNPE, equivalent OLED devices were fabricated with a device architecture of ITO/PEDOT:PSS(60 nm)/2EHO−CNPE(50 nm)/TPBI(40 nm)/Ca(10 nm)/Al(100 nm) in which the emissive layer consists of neat 2EHO−CNPE film prepared by spin-coating. As expected from the solid-state photoluminescence spectra as neat film, the electroluminescence profile of this device showed a red-shifted emission with a peak maxima at ∼473 nm with CIE coordinate of (0.20, 0.15) that is not in the deep-blue region anymore (Figure S11). Furthermore, the optoelectronic performance of this device was found to be much lower (EQE$_{max}$ = 2.36% (at 200 cd/m^2) and CE$_{max}$ = 2.23 cd/A (at 200 cd/m^2)) than those fabricated with the CBP host. This is probably due to more effective confinement of excitons in the emissive layer, more balanced carrier injection/transport, and elimination of undesired molecular aggregation when a proper host material is used.[31] These results clearly show that solution processable hosts with suitable molecular orbital energetics are important for deep-blue color purity and high electroluminescence performance of 2EHO−CNPE, and further improvements could possibly be achieved by using different solution-processable host materials. The charge-transport properties of the new fluorescent molecule were studied by fabricating electron-only and hole-only devices with a configuration of ITO/Al(100 nm)/2EHO−CNPE(50 nm)/Ca(10 nm)/Al(100 nm) and ITO/PEDOT:PSS(60 nm)/2EHO−CNPE(50 nm)/V_2O_5(10 nm)/Al(100 nm), respectively. The electron and hole mobilities were calculated to be 1.5×10^{-5} cm^2/(V s) and 7×10^{-6} cm^2/(V s), respectively, on the basis of the current density−voltage (J−V) characteristics (Figure S12). Although 2EHO−CNPE exhibits ambipolarity with fairly balanced electron and hole transports, slightly better electron-transport ability might reflect the presence of relatively electron-deficient ethynylene and cyano moieties along the molecular π-backbone yielding a highly delocalized LUMO. The observed EQE$_{max}$ for the current 2EHO−CNPE-based electroluminescence is higher than the theoretical limit (EQE = $\gamma\Phi_{PL}\eta_r\eta_{out}$)[31] of ∼5% typically calculated for fluorescent emitters in OLEDs assuming that there is no light-outcoupling enhancing structure ($\eta_{out} \sim 0.2$) and horizontal molecular alignment.[64] Therefore, it is evident that the current molecular design employed in our study could promote a large ratio of radiative singlet exciton formation in the emissive layer, and the radiative exciton yield (η_r) is estimated to be ∼69% (using $\Phi_{PL(CBP:2EHO-CNPE)}$ = 0.51 and γ = 1) that far exceeds the 25% singlet branching ratio based on spin statistics. One should first note that the $T_1 \rightarrow S_0$ conversion, typically observed for phosphorescent molecules, is supposed to be ineffective in this new molecule due to lack of heavy atoms (*weak spin−orbit coupling*). Also, the radiative singlet exciton enhancement is not likely to originate from thermally activated delayed fluorescence (TADF) or triplet−triplet annihilation (TTA) since no delayed fluorescence was observed in the transient PL profile (vide supra); the molecular π-backbone does not adopt a twisted conformation to fully

DOI: 10.1021/acsami.9b12971
ACS Appl. Mater. Interfaces 2019, 11, 44474−44486

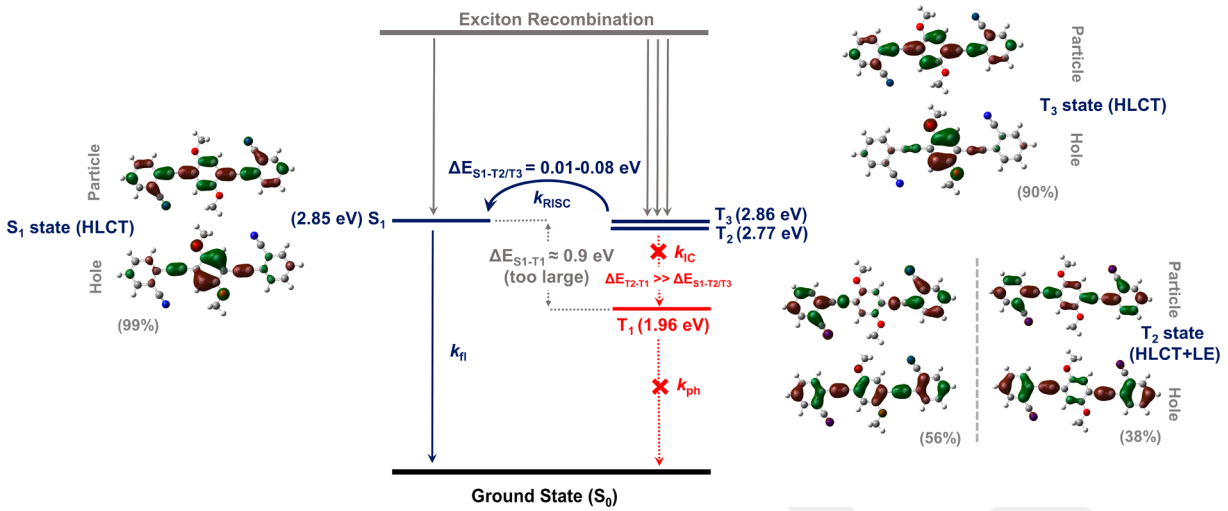

Figure 7. Energy levels and the natural transition orbitals (NTOs) for 2EHO−CNPE excited states calculated with TDDFT in S_0 geometry, and the proposed exciton decay processes (k_{RISC}, reverse intersystem crossing rate; k_{IC}, internal conversion rate; LE, local excited state; HLCT, hybridized local and charge transfer excited state). The weights of each hole−particle pair are given in parentheses.

separate frontier orbitals, the S_1−T_1 energy gap is predicted to be large (vide infra), and the electroluminescence intensity shows a linear relationship with current density.[36,57] Therefore, the observed high η_r could be the result of RISC from high-lying triplet excited states to the first singlet excited state ($T_{(n>1)} \rightarrow S_1$) via hot-exciton process as previously observed for non-TADF donor−acceptor molecules.[65,66]

To further understand the photophysical properties of 2EHO−CNPE and the high radiative exciton ratio in electroluminescence, excited-state energies, oscillator strengths, configurations, and the corresponding natural transition orbitals (NTOs) were calculated with TDDFT (B3LYP/6-311G**) (Figure 7 and Table S3). The calculated energy gap between S_1 and T_1 states is found to be quite large ($\Delta E_{S_1-T_1}$ = 0.89 eV) suggesting an inefficient TADF process for 2EHO−CNPE.[36,37] However, the energies of the high-lying triplet excited states T_2 and T_3 are found to be quite similar to that of the S_1 state ($\Delta E_{S_1-T_3}$= 0.01 eV and $\Delta E_{S_1-T_2}$= 0.08 eV), which could energetically enable hot-exciton processes $T_2 \rightarrow S_1$ and $T_3 \rightarrow S_1$ via RISC. On the other hand, the energy gap between T_2 and T_1 states is found to be as large as 0.81 eV, which, according to the energy gap law, indicates a much lower $T_2 \rightarrow T_1$ internal conversion (IC) rate as compared with the $T_{2/3} \rightarrow S_1$ RISC rate ($k_{RISC} \gg k_{IC}$).[65,67] As clearly seen from the NTO analysis (Figure 7), at least one NTO wave function for each of the S_1, T_2, and T_3 states shows a complete delocalization across the molecular backbone, while its counterpart NTO wave function exhibits a spatial separation. This indicates a good balance of spatial separation (CT) and orbital overlap (LE), showing the coexistence of CT and LE characteristics in the form of HLCT for all of these three excited states. The presence of the CT character in the excited state is particularly key to the conversion of triplet excitons into singlet excitons. Only in the T_2 state there is a pure LE character with a 38% weight. Especially, the configuration of the T_3 excited state is found to be quite similar to the energetically matching S_1 state, which is expected to provide a very effective RISC channel between these states.[65,66,68] The contribution of these high-lying triplet excited states to the luminescence process was also evident in the comparative (ambient vs nitrogen atmosphere) photoluminescence quantum efficiency (Φ_{PL}) measurements. As compared with those recorded under ambient conditions, increased Φ_{PL}s were observed for nitrogen-flushed chloroform solution (Φ_{PL} = 0.90 → 0.95), neat (Φ_{PL} = 0.41 → 0.51), and doped (4:96 wt % 2EHO−CNPE:CBP; Φ_{PL} = 0.51 → 0.58) films under nitrogen atmosphere by using an integrating sphere method. In other words, the reductions in Φ_{PL}s going from nitrogen atmosphere to ambient conditions suggests that the populated high-lying triplet excited states during photoluminescence process are quenched by triplet oxygen when measured under ambient conditions.[36,69] These theoretical results along with the aforementioned photophysical observations clearly suggest that efficient hot-exciton RISC processes between HLCT excited states ($T_{2/3} \rightarrow S_1$) play an important role in the simultaneous harvesting of triplet and singlet excitons ($\eta_r \sim 69\% \gg 25\%$) during electroluminescence. This type of "hot-exciton" process was recently studied for a pure-blue-emitting molecule consisting of phenanthroimidazole, phenylcarbazole, and anthracene units by Ma et al.,[70] which is verified to be a fast process occurring within several nanoseconds. Studies on 2EHO−CNPE's RISC channels via triplet-state sensitization and nanosecond transient absorption spectroscopy will be the subject of future research to provide additional insights into radiative singlet-exciton enhancement mechanism for deep-blue electroluminescence.

CONCLUSIONS

In summary, a new highly soluble A−π−D−π−A-type oligo(*p*-phenyleneethynylene)-based deep-blue emitter, 1,4-bis((2-cyanophenyl)ethynyl)-2,5-bis(2-ethylhexyloxy)benzene (2EHO−CNPE), has been designed and synthesized. The single-crystal structure and thermal, photophysical, and electrochemical properties of the new molecule have been studied in detail. High-photoluminescence quantum efficiencies (Φ_{PL}s) of 0.90 and 0.51 were measured in chloroform solution and as thin film in CBP host, respectively. Intermolecular "C−H···π" and "C−H···N" hydrogen bonding interactions were found to govern the molecular packing in the single-crystal structure without forming π−π stacking. OLEDs exhibited excellent deep-blue electroluminescence (CIE(x,y) = (0.15, 0.09)) with an impressive maximum external quantum

DOI: 10.1021/acsami.9b12971
ACS Appl. Mater. Interfaces 2019, 11, 44474−44486

efficiency of 7.06% (EQE = 6.30% at 200 cd/m^2) and a maximum current efficiency of 5.91 cd/A (CE = 5.34 cd/A at 200 cd/m^2). The experimental results agreed well with the theoretical calculations, and TDDFT calculations indicated that the observed high radiative exciton yield ($\eta_r \sim 69\%$) originates from reverse intersystem crossing processes from the high-lying triplet states to the first singlet excited state ($T_2/T_3 \rightarrow S_1$), all having HLCT characteristics. In addition to showing the first time deep-blue emission of an oligo(*p*-phenyleneethynylene) derivative, the electroluminescence performance shown here is among the highest achieved to date for a deep-blue OLED device in which the emissive layer is solution-processed. The findings presented herein clearly demonstrate that oligo(*p*-phenyleneethynylenes) with proper donor/acceptor functionalizations can play a pronounced role in the development of high-performance deep-blue OLEDs. Furthermore, since oligo(*p*-phenyleneethynylene) offers an extensive π-framework with various positions available to functionalizations, the promising results shown here may stimulate future molecular design efforts for OLEDs. The design rationales presented herein may open up new avenues for the development of fluorescent oligo(*p*-phenyleneethynylenes) with high radiative exciton yields (≫25%) in electroluminescence.

■ ASSOCIATED CONTENT

Supporting Information

The Supporting Information is available free of charge on the ACS Publications website at DOI: 10.1021/acsami.9b12971.

Calculated UV−vis absorption spectrum and molecular orbitals (Figure S1); chemical characterizations (Figures S2−S4); NMR and MALDI TOF-MS spectra (Figures S5−S7); chemical structure (Figure S8); optical absorption/emission (Figure S9) and -photoluminescence spectra (Figure S10); luminance/current density−voltage, current efficiency/external quantum efficiency−current density, and electroluminescence characteristics (Figure S11); *J*−*V* curves (Figure S12); previously reported characteristics (Table S1); crystal data and refinement parameters (Table S2); theoretical excited state data (Table S3) (PDF)

Crystallographic characterizations (CIF)

■ AUTHOR INFORMATION

Corresponding Author

*E-mail: hakan.usta@agu.edu.tr.

ORCID

Hakan Usta: 0000-0002-0618-1979

Resul Ozdemir: 0000-0002-7957-110X

Yunus Zorlu: 0000-0003-2811-1872

Notes

The authors declare no competing financial interest.

■ ACKNOWLEDGMENTS

H.U., S.D., D.A., and E.T. acknowledge support from the Scientific and Technological Research Council of Turkey (TUBITAK), Grant No. 113G035. We thank Prof. Bunyemin Cosut and Prof. Turan Ozturk for their help with the transient photoluminescence decay and quantum efficiency measurements. None of the opinions or determinations in this publication are official opinions of TUBITAK.

■ REFERENCES

(1) Fisher, A. L.; Linton, K. E.; Kamtekar, K. T.; Pearson, C.; Bryce, M. R.; Petty, M. C. Efficient Deep-Blue Electroluminescence from an Ambipolar Fluorescent Emitter in a Single-Active-Layer Device. *Chem. Mater.* **2011**, *23*, 1640−1642.

(2) Zheng, C.-J.; Wang, J.; Ye, J.; Lo, M.-F.; Liu, X.-K.; Fung, M.-K.; Zhang, X.-H.; Lee, C.-S. Novel Efficient Blue Fluorophors with Small Singlet-Triplet Splitting: Hosts for Highly Efficient Fluorescence and Phosphorescence Hybrid WOLEDs with Simplified Structure. *Adv. Mater.* **2013**, *25*, 2205−2211.

(3) Wang, D.; Wu, Z.; Zhang, X.; Jiao, B.; Liang, S.; Wang, D.; He, R.; Hou, X. Solution-Processed Organic Films of Multiple Small-Molecules and White Light-Emitting Diodes. *Org. Electron.* **2010**, *11*, 641−648.

(4) Capelli, R.; Toffanin, S.; Generali, G.; Usta, H.; Facchetti, A.; Muccini, M. Organic Light-Emitting Transistors with an Efficiency That Outperforms the Equivalent Light-Emitting Diodes. *Nat. Mater.* **2010**, *9*, 496−503.

(5) Sun, Y.; Giebink, N. C.; Kanno, H.; Ma, B.; Thompson, M. E.; Forrest, S. R. Management of Singlet and Triplet Excitons for Efficient White Organic Light-Emitting Devices. *Nature* **2006**, *440*, 908−912.

(6) Yang, X.; Xu, X.; Zhou, G. Recent Advances of the Emitters for High Performance Deep-Blue Organic Light-Emitting Diodes. *J. Mater. Chem. C* **2015**, *3*, 913−944.

(7) Lee, D.-H.; Yang, D.; Kim, D.-Y.; Baeg, K.-J. Controlled Ambipolar Charge Transport of Polymer Semiconductors by Viologen-Doping for Complementary-like Electronic Circuits. *Org. Electron.* **2018**, *59*, 224−229.

(8) Lee, D.-H.; Kang, M.; Lim, D.-H.; Kim, Y.; Lee, J.; Kim, D.-Y.; Baeg, K.-J. Simultaneous Enhancement of Charge Density and Molecular Stacking Order of Polymer Semiconductors by Viologen Dopants for High Performance Organic Field-Effect Transistors. *J. Mater. Chem. C* **2018**, *6*, 5497−5505.

(9) Ozdemir, M.; Choi, D.; Kwon, G.; Zorlu, Y.; Kim, H.; Kim, M.-G.; Seo, S.; Sen, U.; Citir, M.; Kim, C.; Usta, H. Design, Synthesis, and Characterization of α,ω-Disubstituted Indeno[1,2-b]Fluorene-6,12-Dione-Thiophene Molecular Semiconductors. Enhancement of Ambipolar Charge Transport through Synthetic Tailoring of Alkyl Substituents. *RSC Adv.* **2016**, *6*, 212−226.

(10) Walker, B.; Tamayo, A. B.; Dang, X.-D.; Zalar, P.; Seo, J. H.; Garcia, A.; Tantiwiwat, M.; Nguyen, T.-Q. Nanoscale Phase Separation and High Photovoltaic Efficiency in Solution-Processed, Small-Molecule Bulk Heterojunction Solar Cells. *Adv. Funct. Mater.* **2009**, *19*, 3063−3069.

(11) Yilmaz, M.; Ozdemir, M.; Erdogan, H.; Tamer, U.; Sen, U.; Facchetti, A.; Usta, H.; Demirel, G. Micro-/Nanostructured Highly Crystalline Organic Semiconductor Films for Surface-Enhanced Raman Spectroscopy Applications. *Adv. Funct. Mater.* **2015**, *25*, 5669−5676.

(12) Demirel, G.; Usta, H.; Yilmaz, M.; Celik, M.; Alidagi, H. A.; Buyukserin, F. Surface-Enhanced Raman Spectroscopy (SERS): An Adventure from Plasmonic Metals to Organic Semiconductors as SERS Platforms. *J. Mater. Chem. C* **2018**, *6*, 5314−5335.

(13) Ozdemir, R.; Choi, D.; Ozdemir, M.; Kwon, G.; Kim, H.; Sen, U.; Kim, C.; Usta, H. Ultralow Bandgap Molecular Semiconductors for Ambient-Stable and Solution-Processable Ambipolar Organic Field-Effect Transistors and Inverters. *J. Mater. Chem. C* **2017**, *5*, 2368−2379.

(14) Facchetti, A. Semiconductors for Organic Transistors. *Mater. Today* **2007**, *10*, 28−37.

(15) Zhang, L.; Colella, N. S.; Cherniawski, B. P.; Mannsfeld, S. C. B.; Briseno, A. L. Oligothiophene Semiconductors: Synthesis, Characterization, and Applications for Organic Devices. *ACS Appl. Mater. Interfaces* **2014**, *6*, 5327−5343.

(16) Lee, S.-H.; Lim, B.; Pei, M.; Yang, H.; Noh, Y.-Y. Highly π-Extended Small Molecules with Bis(Alkylthio)Methylene Side Chains for Organic Field-Effect Transistors. *J. Mater. Chem. C* **2018**, *6*, 7604−7611.

DOI: 10.1021/acsami.9b12971
ACS Appl. Mater. Interfaces 2019, 11, 44474−44486

(17) Ozdemir, R.; Park, S.; Deneme, İ.; Park, Y.; Zorlu, Y.; Alidagi, H. A.; Harmandar, K.; Kim, C.; Usta, H. Triisopropylsilylethynyl-Substituted Indenofluorenes: Carbonyl: Versus Dicyanovinylene Functionalization in One-Dimensional Molecular Crystals and Solution-Processed n-Channel OFETs. *Org. Chem. Front.* **2018**, *5*, 2912−2924.
(18) Jhulki, S.; Mishra, A. K.; Ghosh, A.; Chow, T. J.; Moorthy, J. N. Deep Blue-Emissive Bifunctional (Hole-Transporting + Emissive) Materials with CIE y ∼ 0.06 Based on a 'U'-Shaped Phenanthrene Scaffold for Application in Organic Light-Emitting Diodes. *J. Mater. Chem. C* **2016**, *4*, 9310−9315.
(19) Shan, T.; Liu, Y.; Tang, X.; Bai, Q.; Gao, Y.; Gao, Z.; Li, J.; Deng, J.; Yang, B.; Lu, P.; Ma, Y. Highly Efficient Deep Blue Organic Light-Emitting Diodes Based on Imidazole: Significantly Enhanced Performance by Effective Energy Transfer with Negligible Efficiency Roll-Off. *ACS Appl. Mater. Interfaces* **2016**, *8*, 28771−28779.
(20) Zhou, L.; Yang, L.; Yu, M.; Jiang, Y.; Liu, C.-F.; Lai, W.-Y.; Huang, W. Inkjet-Printed Small-Molecule Organic Light-Emitting Diodes: Halogen-Free Inks, Printing Optimization, and Large-Area Patterning. *ACS Appl. Mater. Interfaces* **2017**, *9*, 40533−40540.
(21) Bail, R.; Hong, J. Y.; Chin, B. D. Inkjet Printing of Blue Phosphorescent Light-Emitting Layer Based on Bis(3,5-Di(9 H -Carbazol-9-Yl))Diphenylsilane. *RSC Adv.* **2018**, *8*, 11191−11197.
(22) Baeg, K.-J.; Caironi, M.; Noh, Y.-Y. Toward Printed Integrated Circuits Based on Unipolar or Ambipolar Polymer Semiconductors. *Adv. Mater.* **2013**, *25*, 4210−4244.
(23) Yan, H.; Chen, Z.; Zheng, Y.; Newman, C.; Quinn, J. R.; Dötz, F.; Kastler, M.; Facchetti, A. A High-Mobility Electron-Transporting Polymer for Printed Transistors. *Nature* **2009**, *457*, 679−686.
(24) Liu, Y.; Zhang, L.; Lee, H.; Wang, H.-W.; Santala, A.; Liu, F.; Diao, Y.; Briseno, A. L.; Russell, T. P. NDI-Based Small Molecule as Promising Nonfullerene Acceptor for Solution-Processed Organic Photovoltaics. *Adv. Energy Mater.* **2015**, *5*, 1500195.
(25) Tang, C. W.; Vanslyke, S. A. Organic Electroluminescent Diodes. *Appl. Phys. Lett.* **1987**, *51*, 913−915.
(26) Ozdemir, M.; Genc, S.; Ozdemir, R.; Altintas, Y.; Citir, M.; Sen, U.; Mutlugun, E.; Usta, H. Trans-Cis Isomerization Assisted Synthesis of Solution-Processable Yellow Fluorescent Maleic Anhydrides for White-Light Generation. *Synth. Met.* **2015**, *210*, 192−200.
(27) Jou, J.; Kumar, S.; Fang, P.; Venkateswararao, A.; Thomas, K. R. J.; Shyue, J.-J.; Wang, Y.-C.; Li, T.-H.; Yu, H.-H. Highly Efficient Ultra-Deep Blue Organic Light-Emitting Diodes with a Wet- and Dry-Process Feasible Cyanofluorene Acetylene Based Emitter. *J. Mater. Chem. C* **2015**, *3*, 2182−2194.
(28) Liu, C.; Li, Y.; Zhang, Y.; Yang, C.; Wu, H.; Qin, J.; Cao, Y. Solution-Processed, Undoped, Deep-Blue Organic Light-Emitting Diodes Based on Starburst Oligofluorenes with a Planar Triphenylamine Core. *Chem. -Eur. J.* **2012**, *18*, 6928−6934.
(29) Li, Y.; Gao, S.; Zhang, N.; Huang, X.; Tian, J.; Xu, F.; Sun, Z.; Yin, S.; Wu, X.; Chu, W. Solution-Processable, High Luminance Deep-Blue Organic Light Emitting Devices Based on Novel Naphthalene Bridged Bis-Triphenylamine Derivatives. *J. Mater. Chem. C* **2019**, *7*, 2686−2698.
(30) Huang, H.; Fu, Q.; Zhuang, S.; Liu, Y.; Wang, L.; Chen, J.; Ma, D.; Yang, C. Novel Deep Blue OLED Emitters with 1,3,5-Tri(Anthracen-10-Yl)Benzene-Centered Starburst Oligofluorenes. *J. Phys. Chem. C* **2011**, *115*, 4872−4878.
(31) Jou, J. H.; Li, J. L.; Sahoo, S.; Dubey, D. K.; Kumar Yadav, R. A.; Joseph, V.; Thomas, K. R. J.; Wang, C. W.; Jayakumar, J.; Cheng, C. H. Enabling a 6.5% External Quantum Efficiency Deep-Blue Organic Light-Emitting Diode with a Solution-Processable Carbazole-Based Emitter. *J. Phys. Chem. C* **2018**, *122*, 24295−24303.
(32) Maciejczyk, M. R.; Zhang, S.; Hedley, G. J.; Robertson, N.; Samuel, I. D. W.; Pietraszkiewicz, M. Monothiatruxene-Based, Solution-Processed Green, Sky-Blue, and Deep-Blue Organic Light-Emitting Diodes with Efficiencies Beyond 5% Limit. *Adv. Funct. Mater.* **2019**, *29*, 1807572.
(33) Reddy, S. S.; Sree, V. G.; Gunasekar, K.; Cho, W.; Gal, Y.-S.; Song, M.; Kang, J.-W.; Jin, S.-H. Highly Efficient Bipolar Deep-Blue Fluorescent Emitters for Solution-Processed Non-Doped Organic Light-Emitting Diodes Based on 9,9-Dimethyl-9,10-Dihydroacridine/Phenanthroimadazole Derivatives. *Adv. Opt. Mater.* **2016**, *4*, 1236−1246.
(34) Liu, C.; Fu, Q.; Zou, Y.; Yang, C.; Ma, D.; Qin, J. Low Turn-on Voltage, High-Power-Efficiency, Solution-Processed Deep-Blue Organic Light-Emitting Diodes Based on Starburst Oligofluorenes with Diphenylamine End-Capper to Enhance the HOMO Level. *Chem. Mater.* **2014**, *26*, 3074−3083.
(35) Zhang, J.; Ding, D.; Wei, Y.; Xu, H. Extremely Condensing Triplet States of DPEPO-Type Hosts through Constitutional Isomerization for High-Efficiency Deep-Blue Thermally Activated Delayed Fluorescence Diodes. *Chem. Sci.* **2016**, *7*, 2870−2882.
(36) Jürgensen, N.; Kretzschmar, A.; Höfle, S.; Freudenberg, J.; Bunz, U. H. F.; Hernandez-Sosa, G. Sulfone-Based Deep Blue Thermally Activated Delayed Fluorescence Emitters: Solution-Processed Organic Light-Emitting Diodes with High Efficiency and Brightness. *Chem. Mater.* **2017**, *29*, 9154−9161.
(37) Uoyama, H.; Goushi, K.; Shizu, K.; Nomura, H.; Adachi, C. Highly Efficient Organic Light-Emitting Diodes from Delayed Fluorescence. *Nature* **2012**, *492*, 234−238.
(38) Xu, H.; Chen, R.; Sun, Q.; Lai, W.; Su, Q.; Huang, W.; Liu, X. Recent Progress in Metal−Organic Complexes for Optoelectronic Applications. *Chem. Soc. Rev.* **2014**, *43*, 3259−3302.
(39) Wong, M. Y.; Krotkus, S.; Copley, G.; Li, W.; Murawski, C.; Hall, D.; Hedley, G. J.; Jaricot, M.; Cordes, D. B.; Slawin, A. M. Z.; Olivier, Y.; Beljonne, D.; Muccioli, L.; Moral, M.; Sancho-Garcia, J.-C.; Gather, M. C.; Samuel, I. D. W.; Zysman-Colman, E. Deep-Blue Oxadiazole-Containing Thermally Activated Delayed Fluorescence Emitters for Organic Light-Emitting Diodes. *ACS Appl. Mater. Interfaces* **2018**, *10*, 33360−33372.
(40) Zhang, Q.; Li, J.; Shizu, K.; Huang, S.; Hirata, S.; Miyazaki, H.; Adachi, C. Design of Efficient Thermally Activated Delayed Fluorescence Materials for Pure Blue Organic Light Emitting Diodes. *J. Am. Chem. Soc.* **2012**, *134*, 14706−14709.
(41) Fleetham, T.; Li, G.; Wen, L.; Li, J. Efficient "Pure" Blue OLEDs Employing Tetradentate Pt Complexes with a Narrow Spectral Bandwidth. *Adv. Mater.* **2014**, *26*, 7116−7121.
(42) Li, G.; Fleetham, T.; Turner, E.; Hang, X.-C.; Li, J. Highly Efficient and Stable Narrow-Band Phosphorescent Emitters for OLED Applications. *Adv. Opt. Mater.* **2015**, *3*, 390−397.
(43) Lee, J.; Chen, H.-F.; Batagoda, T.; Coburn, C.; Djurovich, P. I.; Thompson, M. E.; Forrest, S. R. Deep Blue Phosphorescent Organic Light-Emitting Diodes with Very High Brightness and Efficiency. *Nat. Mater.* **2016**, *15*, 92−98.
(44) Kondo, Y.; Yoshiura, K.; Kitera, S.; Nishi, H.; Oda, S.; Gotoh, H.; Sasada, Y.; Yanai, M.; Hatakeyama, T. Narrowband Deep-Blue Organic Light-Emitting Diode Featuring an Organoboron-Based Emitter. *Nat. Photonics* **2019**, *13*, 678−682.
(45) Chan, C.; Cui, L.; Kim, J. U.; Nakanotani, H.; Adachi, C. Rational Molecular Design for Deep-Blue Thermally Activated Delayed Fluorescence Emitters. *Adv. Funct. Mater.* **2018**, *28*, 1706023.
(46) Wada, Y.; Kubo, S.; Kaji, H. Adamantyl Substitution Strategy for Realizing Solution-Processable Thermally Stable Deep-Blue Thermally Activated Delayed Fluorescence Materials. *Adv. Mater.* **2018**, *30*, 1705641.
(47) Zhao, L.; Perepichka, I. F.; Türksoy, F.; Batsanov, A. S.; Beeby, A.; Findlay, K. S.; Bryce, M. R. 2,5-Di(Aryleneethynyl)Pyrazine Derivatives: Synthesis, Structural and Optoelectronic Properties, and Light-Emitting Device. *New J. Chem.* **2004**, *28*, 912−918.
(48) Mao, G.; Orita, A.; Fenenko, L.; Yahiro, M.; Adachi, C.; Otera, J. Blue Emitting Fluorophores of Phenyleneethynylenes Substituted by Diphenylethenyl Terminal Groups for Organic Light-Emitting Diodes. *Mater. Chem. Phys.* **2009**, *115*, 378−384.
(49) Fenenko, L.; Shao, G.; Orita, A.; Yahiro, M.; Otera, J.; Svechnikov, S.; Adachi, C. Electrical Properties of 1,4-Bis(4-(Phenylethynyl)Phenylethynyl)Benzene and Its Application for Organic Light Emitting Diodes. *Chem. Commun.* **2007**, 2278−2280.

DOI: 10.1021/acsami.9b12971
ACS Appl. Mater. Interfaces 2019, 11, 44474−44486

(50) Ervithayasuporn, V.; Abe, J.; Wang, X.; Matsushima, T.; Murata, H.; Kawakami, Y. Synthesis, Characterization, and OLED Application of Oligo(p-Phenylene Ethynylene)s with Polyhedral Oligomeric Silsesquioxanes (POSS) as Pendant Groups. *Tetrahedron* **2010**, *66*, 9348−9355.
(51) Yamaguchi, Y.; Ochi, T.; Miyamura, S.; Tanaka, T.; Kobayashi, S.; Wakamiya, T.; Matsubara, Y.; Yoshida, Z. I. Rigid Molecular Architectures That Comprise a 1,3,5-Trisubstituted Benzene Core and Three Oligoaryleneethynylene Arms: Light-Emitting Characteristics and π Conjugation between the Arms. *J. Am. Chem. Soc.* **2006**, *128*, 4504−4505.
(52) Yamaguchi, Y.; Matsubara, Y.; Ochi, T.; Wakamiya, T.; Yoshida, Z. I. How the π Conjugation Length Affects the Fluorescence Emission Efficiency. *J. Am. Chem. Soc.* **2008**, *130*, 13867−13869.
(53) Ochi, T.; Yamaguchi, Y.; Wakamiya, T.; Matsubara, Y.; Yoshida, Z. I. Block Modification of Rod-Shaped π Conjugated Carbon Frameworks with Donor and Acceptor Groups toward Highly Fluorescent Molecules: Synthesis and Emission Characteristics. *Org. Biomol. Chem.* **2008**, *6*, 1222−1231.
(54) Thomas, R.; Varghese, S.; Kulkarni, G. U. The Influence of Crystal Packing on the Solid State Fluorescence Behavior of Alkyloxy Substituted Phenyleneethynylenes. *J. Mater. Chem.* **2009**, *19*, 4401−4406.
(55) Yamaguchi, Y.; Ochi, T.; Matsubara, Y.; Yoshida, Z. Highly Emissive Whole Rainbow Fluorophores Consisting of 1,4-Bis(2-Phenylethynyl)Benzene Core Skeleton: Design, Synthesis, and Light-Emitting Characteristics. *J. Phys. Chem. A* **2015**, *119*, 8630−8642.
(56) Frisch, M. J.; Trucks, G. W.; Schlegel, H. B.; Scuseria, G. E.; Robb, M. A.; Cheeseman, J. R.; Scalmani, G.; Barone, V.; Mennucci, B.; Petersson, G. A.; Nakatsuji, H.; Caricato, M.; Li, X.; Hratchian, H. P.; Izmaylov, A. F.; Bloino, J.; Zheng, G.; Sonnenberg, J. L.; Hada, M.; Ehara, M.; Toyota, K.; Fukuda, R.; Hasegawa, J.; Ishida, M.; Nakajima, T.; Honda, Y.; Kitao, O.; Nakai, H.; Vreven, T.; Montgomery, J. A., Jr.; Peralta, J. E.; Ogliaro, F.; Bearpark, M.; Heyd, J. J.; Brothers, E.; Kudin, K. N.; Staroverov, V. N.; Keith, T.; Kobayashi, R.; Normand, J.; Raghavachari, K.; Rendell, A.; Burant, J. C.; Iyengar, S. S.; Tomasi, J.; Cossi, M.; Rega, N.; Millam, J. M.; Klene, M.; Knox, J. E.; Cross, J. B.; Bakken, V.; Adamo, C.; Jaramillo, J.; Gomperts, R.; Stratmann, R. E.; Yazyev, O.; Austin, A. J.; Cammi, R.; Pomelli, C.; Ochterski, J. W.; Martin, R. L.; Morokuma, K.; Zakrzewski, V. G.; Voth, G. A.; Salvador, P.; Dannenberg, J. J.; Dapprich, S.; Daniels, A. D.; Farkas, O.; Foresman, J. B.; Ortiz, J. V.; Cioslowski, J.; Fox, D. J. *Gaussian 09*, Revision C.01; Gaussian: Wallingford, CT, USA, 2010.
(57) Tang, X.; Bai, Q.; Peng, Q.; Gao, Y.; Li, J.; Liu, Y.; Yao, L.; Lu, P.; Yang, B.; Ma, Y. Efficient Deep Blue Electroluminescence with an External Quantum Efficiency of 6.8% and CIE y < 0.08 Based on a Phenanthroimidazole−Sulfone Hybrid Donor−Acceptor Molecule. *Chem. Mater.* **2015**, *27*, 7050−7057.
(58) Li, W.; Pan, Y.; Yao, L.; Liu, H.; Zhang, S.; Wang, C.; Shen, F.; Lu, P.; Yang, B.; Ma, Y. A Hybridized Local and Charge-Transfer Excited State for Highly Efficient Fluorescent OLEDs: Molecular Design, Spectral Character, and Full Exciton Utilization. *Adv. Opt. Mater.* **2014**, *2*, 892−901.
(59) Zhen, C.-G.; Chen, Z.-K.; Liu, Q.-D.; Dai, Y.-F.; Shin, R. Y. C.; Chang, S.-Y.; Kieffer, J. Fluorene-Based Oligomers for Highly Efficient and Stable Organic Blue-Light-Emitting Diodes. *Adv. Mater.* **2009**, *21*, 2425−2429.
(60) Li, H.; Powell, D. R.; Hayashi, R. K.; West, R. Poly((2,5-dialkoxy-p-phenylene)ethynylene -p -phenyleneethynylene)s and Their Model Compounds. *Macromolecules* **1998**, *31*, 52−58.
(61) Furniss, B. S.; Hannaford, A. J.; Smith, P. W. G.; Tatchell, A. R. *Vogel's Textbook of Practical Organic Chemistry*, 5th ed.; Wiley-VCH Verlag: New York, 1989.
(62) Lide, D. R. *CRC Handbook of Chemistry and Physics*, 87th ed.; Taylor and Francis: Boca Raton, FL, USA, 2007.
(63) Li, W.; Liu, D.; Shen, F.; Ma, D.; Wang, Z.; Feng, T.; Xu, Y.; Yang, B.; Ma, Y. A Twisting Donor-Acceptor Molecule with an Intercrossed Excited State for Highly Efficient, Deep-Blue Electroluminescence. *Adv. Funct. Mater.* **2012**, *22*, 2797−2803.
(64) Schmidt, T. D.; Lampe, T.; Sylvinson, M. R. D.; Djurovich, P. I.; Thompson, M. E.; Brütting, W. Emitter Orientation as a Key Parameter in Organic Light-Emitting Diodes. *Phys. Rev. Appl.* **2017**, *8*, 037001.
(65) Yao, L.; Zhang, S.; Wang, R.; Li, W.; Shen, F.; Yang, B.; Ma, Y. Highly Efficient Near-Infrared Organic Light-Emitting Diode Based on a Butterfly-Shaped Donor-Acceptor Chromophore with Strong Solid-State Fluorescence and a Large Proportion of Radiative Excitons. *Angew. Chem., Int. Ed.* **2014**, *53*, 2119−2123.
(66) Zhang, S.; Yao, L.; Peng, Q.; Li, W.; Pan, Y.; Xiao, R.; Gao, Y.; Gu, C.; Wang, Z.; Lu, P.; Li, F.; Su, S.; Yang, B.; Ma, Y. Achieving a Significantly Increased Efficiency in Nondoped Pure Blue Fluorescent OLED: A Quasi-Equivalent Hybridized Excited State. *Adv. Funct. Mater.* **2015**, *25*, 1755−1762.
(67) Turro, N. J. *Modern Molecular Photochemistry*; University Science Books: Sausalito, CA, USA, 1991.
(68) Ouyang, X.; Li, X.-L.; Ai, L.; Mi, D.; Ge, Z.; Su, S.-J. Novel "Hot Exciton" Blue Fluorophores for High Performance Fluorescent/Phosphorescent Hybrid White Organic Light-Emitting Diodes with Superhigh Phosphorescent Dopant Concentration and Improved Efficiency Roll-Off. *ACS Appl. Mater. Interfaces* **2015**, *7*, 7869−7877.
(69) Yang, Z.; Mao, Z.; Xie, Z.; Zhang, Y.; Liu, S.; Zhao, J.; Xu, J.; Chi, Z.; Aldred, M. P. Recent Advances in Organic Thermally Activated Delayed Fluorescence Materials. *Chem. Soc. Rev.* **2017**, *46*, 915−1016.
(70) Xu, Y.; Liang, X.; Zhou, X.; Yuan, P.; Zhou, J.; Wang, C.; Li, B.; Hu, D.; Qiao, X.; Jiang, X.; Liu, L.; Su, S.-J.; Ma, D.; Ma, Y. Highly Efficient Blue Fluorescent OLEDs Based on Upper Level Triplet−Singlet Intersystem Crossing. *Adv. Mater.* **2019**, *31*, 1807388.

DOI: 10.1021/acsami.9b12971
ACS Appl. Mater. Interfaces 2019, 11, 44474−44486